Supporting Information

Atomic Resolution Monitoring of Cation Exchange in CdSe-PbSe Hetero-Nanocrystals during Epitaxial Solid-Solid-Vapor Growth

Anil O. Yalcin[1,‡], Zhaochuan Fan[2,‡], Bart Goris[3], Wun-Fan Li[4], Rik S. Koster[4], Chang-Ming Fang[4], Alfons van Blaaderen[4], Marianna Casavola[5], Frans D. Tichelaar[1], Sara Bals[3], Gustaaf Van Tendeloo[3], Thijs J.H. Vlugt[2], Daniël Vanmaekelbergh[5], Henny W. Zandbergen[1], Marijn A. van Huis[4,1,]*

[1] Kavli Institute of Nanoscience, Delft University of Technology,
Lorentzweg 1, 2628 CJ Delft, The Netherlands
[2] Process and Energy Laboratory, Delft University of Technology,
Leeghwaterstraat 39, 2628 CB Delft, The Netherlands
[3] Electron Microscopy for Materials Science (EMAT), University of Antwerp,
Groenenborgerlaan 171, 2020 Antwerp, Belgium
[4] Soft Condensed Matter, Debye Institute for Nanomaterials Science, Utrecht University,
Princetonplein 5, 3584 CC Utrecht, The Netherlands
[5] Condensed Matter and Interfaces, Debye Institute for Nanomaterials Science, Utrecht University,
Princetonplein 5, 3584 CC Utrecht, The Netherlands
‡These authors contributed equally.

[*] E-mail: m.a.vanhuis@uu.nl

Supporting Information Contents

A. Supporting movies

In general, a heating rate of 10 degrees/min was used and when reaching the specified temperature, the HNCs were annealed for 5 min at constant temperature.

Movie S1. HAADF-STEM movie of the change observed from **Figure 1b** to **Figure 1c**, where two dumbbell morphology HNCs (CdSe nanorod with PbSe tips) turned totally to a brighter PbSe contrast with heating from 160 ^{0}C to 200 ^{0}C. Movie S1 was accelerated 20 times.

Movies S2. HAADF-STEM movie, where a dumbbell morphology NC turned totally to a brighter PbSe contrast with heating from 200 ^{0}C to 210 ^{0}C. STEM-EDX elemental maps of this dumbbell NC after transformation are given in **Figure S4**. Movie S2 was accelerated 10 times.

Movie S3. HAADF-STEM movie, where a dumbbell morphology was half covered with PbSe brighter contrast. Further heating led to sublimation of first CdSe nanorod domain (not transformed part) and then slowly PbSe domains. This movie shows that when there is not enough Pb-source, the cation exchange cannot proceed. The HNC was heated from 190 ^{0}C to 210 ^{0}C. Supporting Movie S3 was accelerated 20 times.

Movie S4. High resolution HAADF-STEM movie of **Figure 2a** and **Figure 2b**, where the CdSe nanorod domain transformed partially from hexagonal wurtzite to the PbSe cubic rock-salt structure with heating from 160 ^{0}C to 180 ^{0}C. Movie S4 was accelerated 20 times.

B. Schematic of the atomistic growth mechanism

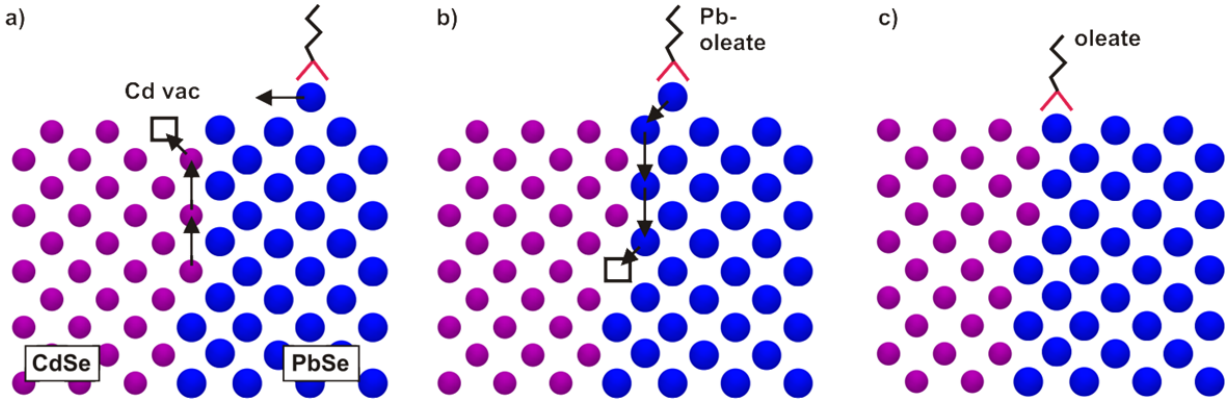

Figure S1. Schematic depicting the cation exchange process. Only the Cd, Pb atomic species are shown. (a) After a Cd vacancy is formed at the CdSe surface, it will diffuse at the CdSe side of the CdSe/PbSe interface. (b) The cation exchange step takes place when a Pb atoms from the other side of the interface jumps into the vacant Cd site. The Pb vacancy which is thereby formed will diffuse to the PbSe surface, where it recombines with the Pb from an adsorbed Pb-oleate molecule. (c) The oleate molecule remains adsorbed at the HNC surface.

C. Synthesis of the PbSe/CdSe dumbbells

Chemicals. Cadmium oxide (CdO, 99.99%), tri-n-octylphosphine oxide (TOPO, 99%), tri-octyl-phosphine (TOP, 90%), selenium powder (98%), diphenyl ether (DPE, 99%), oleic acid (OLAC, 90%) and lead(II) acetate trihydrate (99.95%) were purchased from Sigma Aldrich; n-tetradecylphosphonic acid (TDPA) and n-hexylphosphonic acid (HPA) were purchased from PolyCarbon Industries.

Synthesis of the CdSe nanorods. The synthesis of CdSe nanorods was performed according to the procedure published by Gur et al. [1] and Peng et al. [2]. In a typical synthesis 0.2 g cadmium oxide, 0.71 g of n-tetradecylphosphonic acid, 0.16 g n-hexylphosphonic acid and 3 g of tri-n-octylphosphine oxide are loaded in 50 ml flask. The mixture is heated to 120 ° C in nitrogen atmosphere and then kept at 120 ° C under vacuum for one hour. The mixture is successively heated up to 300 ° C under nitrogen for about 30 minutes to allow CdO to dissolve. The mixture is then heated up to 310 ° C and 1.5 g of trioctylphosphine (TOP) are injected. When the temperature recovers to 310 ° C, a solution of selenium in TOP (0.073g Se +

0.416 g TOP) is rapidly injected and the reaction is allowed to proceed at a constant temperature of 310 º C for 7 minutes. The reaction is finally quenched by fast removal of the heating source. The nanoparticle suspension is allowed to cool down and at about 50 º C and 2.5 ml of anhydrous toluene are added. The nanorod suspension is purified by three cycles of precipitation in isopropanol, centrifugation and re-dispersion in toluene.

Synthesis of the CdSe-PbSe heterostructures. PbSe-tipped CdSe nanorod heterostructured nanocrystals have been synthesized according to the method published by Kudera et al. [3] and Carbone et al. [4] with slight modifications. A stock solution of lead oleate is prepared by degassing 2 mL diphenyl ether (DPE), 1.5 mL oleic acid and 1.7 mmol Lead(II)acetate for 2 hours at 120 º C. The solution is cooled to room temperature and then transferred and stored in a nitrogen-filled glovebox. For the heterostructures preparation, 5 ml diphenyl ether are degassed under vacuum at 120 º C for about 30 minutes. The degassed solvent is then allowed to cool down to about 50 º C and 0.3 ml of a suspension of CdSe nanorods are injected under nitrogen atmosphere. The suspension of nanorods in DPE is then heated up to 130 º C under nitrogen atmosphere. Then, a mixture of precursors is prepared in a nitrogen filled glovebox by mixing 0.75 ml of lead oleate stock solution with 0.45 ml TOP and 0.3 ml of a Se-TOP solution (1M). This solution, containing both the Pb and Se precursors in a 1:1 proportion, is then drop-wise injected in the CdSe/DPE suspension at 130 º C via a syringe pump at a rate of 0.1 ml/min. Once all the precursor solution has been injected the temperature is kept at 130 º C for additional 3 minutes. The suspension is then allowed to cool down to room temperature and it is transferred in the glovebox. The CdSe-PbSe nanocrystals are purified by three cycles of precipitation of the suspension in butanol/methanol, centrifugation and re-dispersion in toluene.

D. Supporting TEM images and chemical mapping

Table S1. Chemical composition of nanodomains (quantification of STEM-EDX maps using the Cliff-Lorimer method). More details can be found in the Supporting information, in Figures S5-S19 and Tables S2-S6.

	Pb (at. %)	Se (at. %)	Cd (at. %)	cation/anion ratio
PbSe tips at initial state	51 ± 6	43 ± 5	6 ± 4	1.3 ± 0.2
PbSe tips from where cation exchange proceeded to certain extent	44 ± 3	49 ± 5	7 ± 4	1.02 ± 0.14
Nanorod domains where partial cation exchange took place	42 ± 5	52 ± 2	6 ± 3	0.93 ± 0.11
PbSe tips of nanorods where total cation exchange was observed	46 ± 2	51 ± 3	3 ± 3	0.94 ± 0.10
Nanorod domains where total cation exchange was observed	46 ± 2	51 ± 3	3 ± 3	0.97 ± 0.09

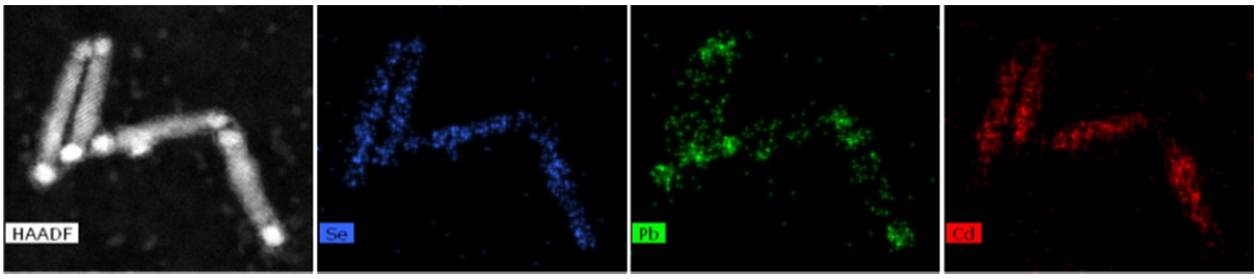

Figure S2. STEM-EDX elemental maps of dumbbell morphologies in initial state. Elemental maps show clearly that the morphology is CdSe nanorod with PbSe tips.

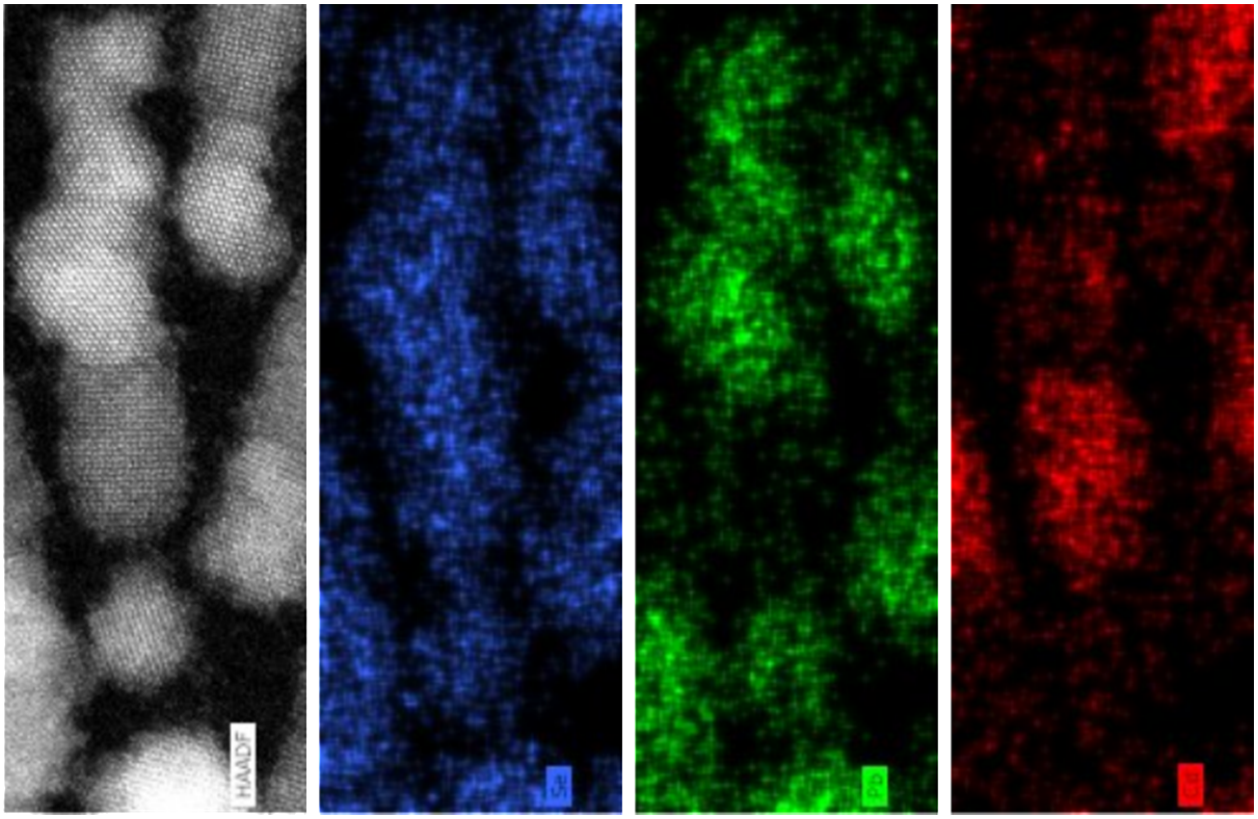

Figure S3. STEM-EDX elemental maps of dumbbell morphology NC where PbSe contrast has propagated into half of the CdSe nanorod. Elemental maps show that the bright contrast CdSe nanorod domain has become PbSe through cation exchange.

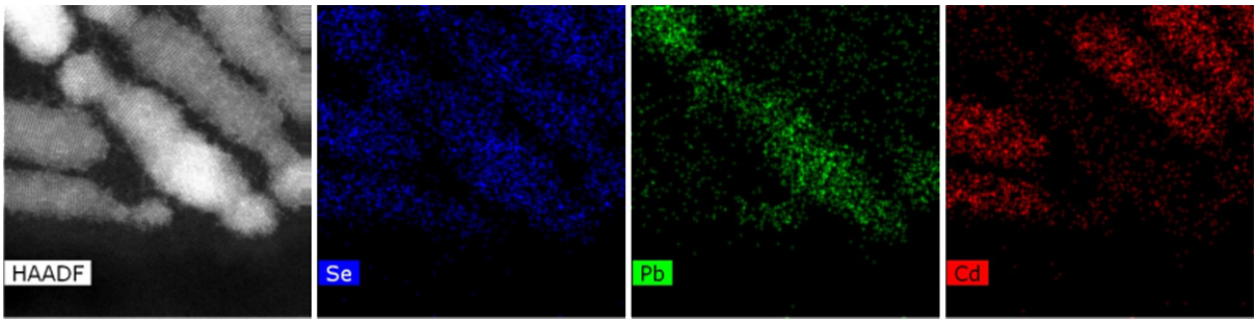

Figure S4. STEM-EDX elemental maps of dumbbell structure (shown in **Movie S2**) after full cation exchange. The whole CdSe nanorod transformed to PbSe domain.

Chemi-STEM Quantitative Elemental Analysis (Table 1 Data)

Dumbbell Morphology NCs in Initial State: Figure S5-S10. The quantitative analyses were carried out the yellow highlighted regions with numbers. STEM-EDX quantification data of 18 PbSe tips (Figure S5-S10) in dumbbell NCs at the initial state are shown in Table S2.

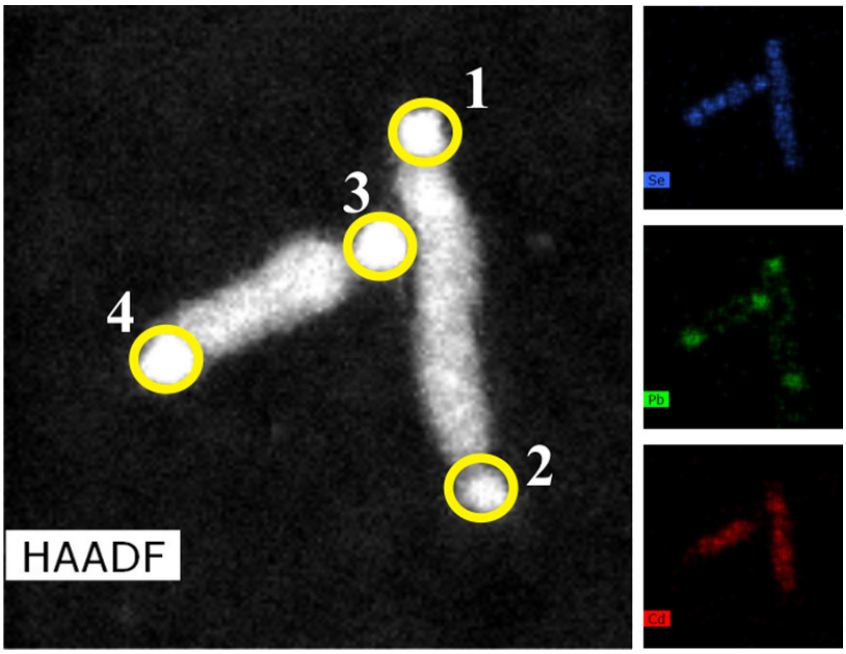

Atomic percentages:

- **Region 1: PbSe tip**
  - **Pb: 46.28**
  - **Se: 45.61**
  - **Cd: 8.10**
- **Region 2: PbSe tip**
  - **Pb: 63.44**
  - **Se: 35.17**
  - **Cd: 1.39**
- **Region 3: PbSe tip**
  - **Pb: 50.31**
  - **Se: 47.11**
  - **Cd: 2.58**
- **Region 4: PbSe tip**
  - **Pb: 43.82**
  - **Se: 48.71**
  - **Cd: 7.47**

Figure S5: CdSe-PbSe dumbbell NCs in the initial state.

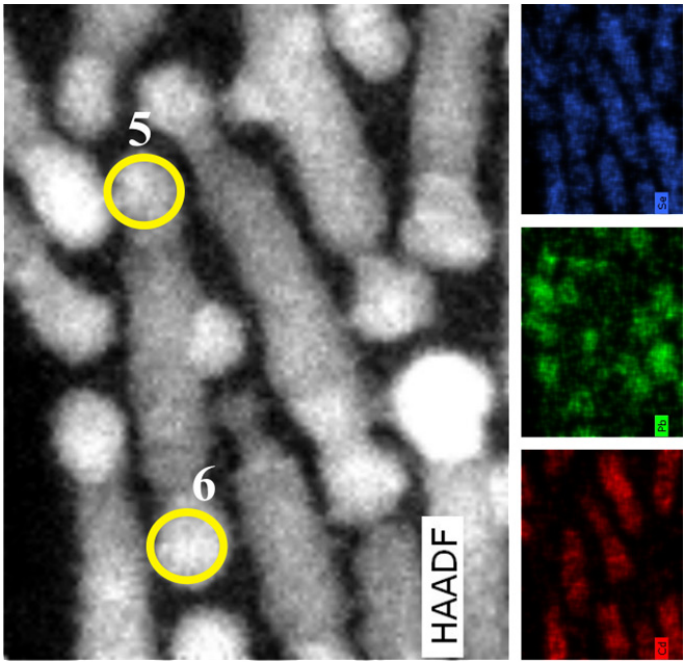

Atomic percentages:

- **Region 5: PbSe tip**
  - **Pb: 45.17**
  - **Se: 51.5**
  - **Cd: 3.33**
- **Region 6: PbSe tip**
  - **Pb: 44.18**
  - **Se: 48.08**
  - **Cd: 7.74**
- **Region 7: PbSe tip**
  - **Pb: 49.08**
  - **Se: 48.15**
  - **Cd: 2.77**

Figure S6: CdSe-PbSe dumbbell NC in the initial state.

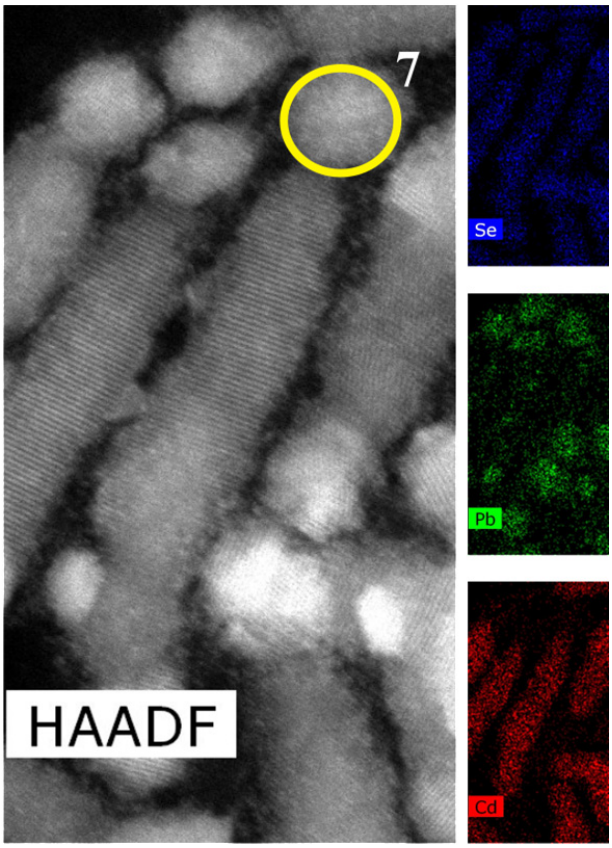

Figure S7. CdSe-PbSe dumbbell NC in the initial state.

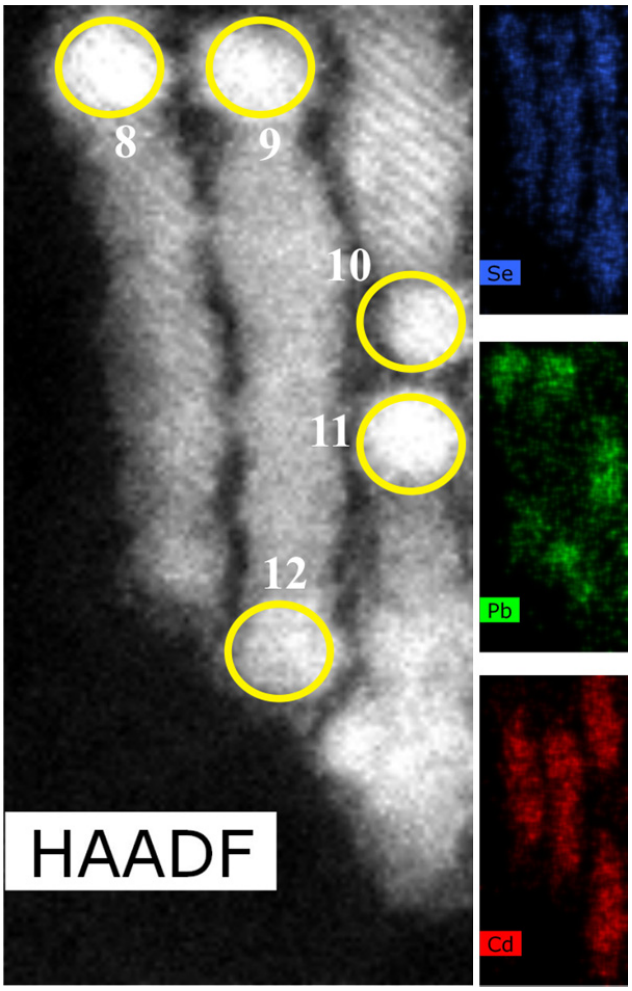

Atomic percentages:

- **Region 8: PbSe tip**
  - **Pb: 49.06**
  - **Se: 42.28**
  - **Cd: 8.66**
- **Region 9: PbSe tip**
  - **Pb: 48.65**
  - **Se: 42.36**
  - **Cd: 8.99**
- **Region 10: PbSe tip**
  - **Pb: 46.59**
  - **Se: 38.66**
  - **Cd: 14.74**
- **Region 11: PbSe tip**
  - **Pb: 58.76**
  - **Se: 34.28**
  - **Cd: 6.96**
- **Region 12: PbSe tip**
  - **Pb: 45.49**
  - **Se: 43.18**
  - **Cd: 11.33**

Figure S8. CdSe-PbSe dumbbell NCs in the initial state.

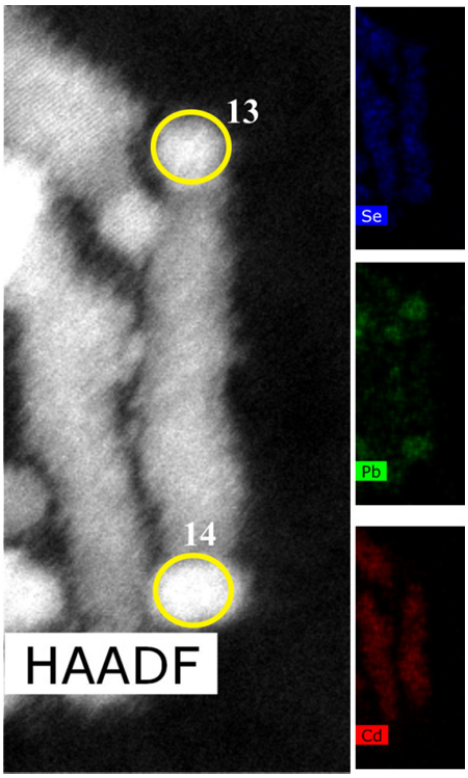

Figure S9. CdSe-PbSe dumbbell NC in the initial state.

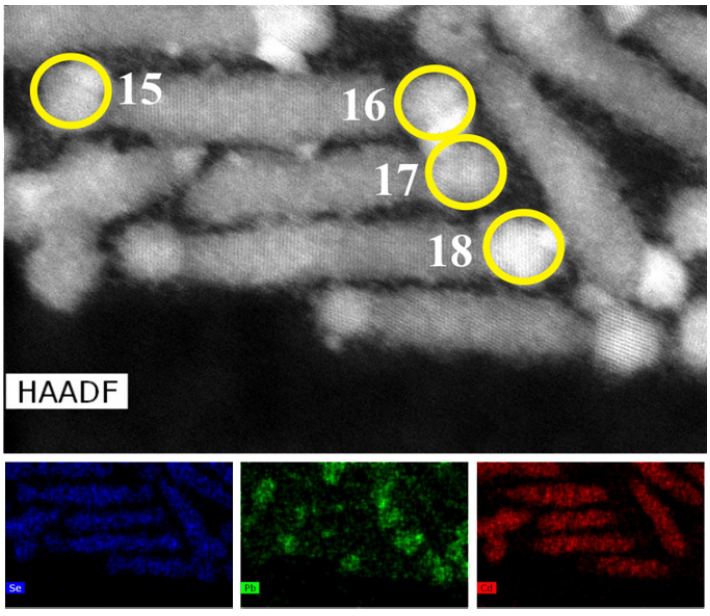

Figure S10. CdSe-PbSe dumbbell NCs in the initial state.

Atomic percentages:

- **Region 13: PbSe tip**
  - **Pb: 59.35**
  - **Se: 38.81**
  - **Cd: 1.84**
- **Region 14: PbSe tip**
  - **Pb: 46.30**
  - **Se: 48.65**
  - **Cd: 5.05**
- **Region 15: PbSe tip**
  - **Pb: 44.86**
  - **Se: 46.53**
  - **Cd: 8.60**
- **Region 16: PbSe tip**
  - **Pb: 62.03**
  - **Se: 33.01**
  - **Cd: 4.96**
- **Region 17: PbSe tip**
  - **Pb: 53.15**
  - **Se: 43.21**
  - **Cd: 3.65**
- **Region 18: PbSe tip**
  - **Pb: 53.33**
  - **Se: 45.52**
  - **Cd: 1.15**

Table S2. Quantification data of 18 STEM-EDX studies on PbSe tips (Figure S5-S10) of dumbbell NCs in the initial state.

PbSe tips at initial state			
	Pb (%)	**Se (%)**	**Cd (%)**
Region 1	46.28	45.61	8.1
Region 2	63.44	35.17	1.39
Region 3	50.31	47.11	2.58
Region 4	43.82	48.71	7.47
Region 5	45.17	51.5	3.33
Region 6	44.18	48.08	7.74
Region 7	49.08	48.15	2.77
Region 8	49.06	42.28	8.66
Region 9	48.65	42.36	8.99
Region 10	46.59	38.66	14.74
Region 11	58.76	34.28	6.96
Region 12	45.49	43.18	11.33
Region 13	59.35	38.81	1.84
Region 14	46.3	48.65	5.05
Region 15	44.86	46.53	8.6
Region 16	62.03	33.01	4.96
Region 17	53.15	43.21	3.65
Region 18	53.33	45.52	1.15
Mean	50.55	43.38	6.07
Standard Deviation	6.37	5.44	3.73

NCs whereby the cation exchange reaction proceeded along the CdSe nanorod: Figures S11-S16. The quantitative analyses were carried out the yellow highlighted regions with numbers. STEM-EDX quantification data of 10 PbSe tips (Figure S11-S16) from where cation exchange proceeded are shown in Table S3. STEM-EDX quantification data of 10 nanorod domains (Figures S11-S16) where cation exchange took place are shown in Table S4.

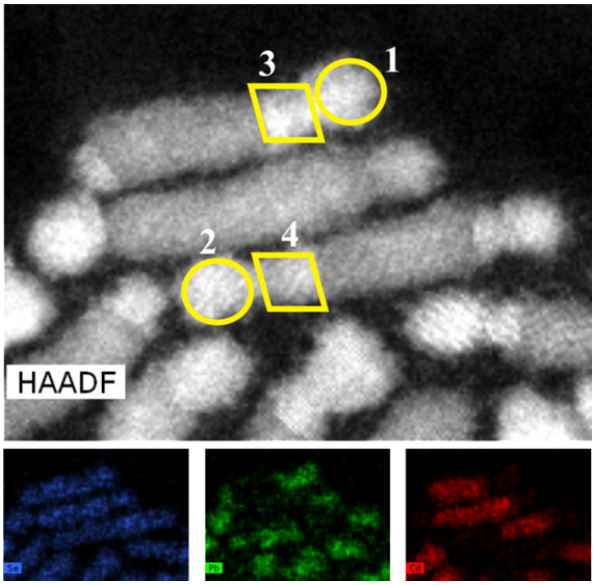

Figure S11. CdSe-PbSe dumbbell NCs where some cation exchange was observed.

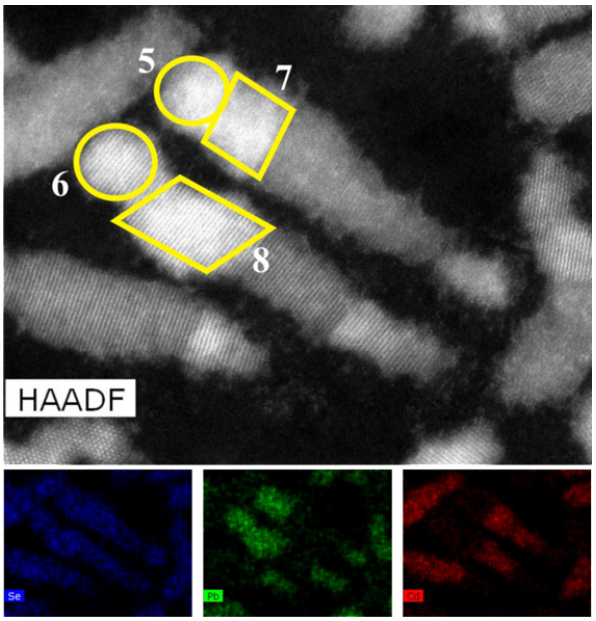

Figure S12. CdSe-PbSe dumbbell NCs where some cation exchange was observed.

Atomic percentages:

- **Region 1: PbSe tip**
  - **Pb: 41.04**
  - **Se: 45.77**
  - **Cd: 13.19**
- **Region 2: PbSe tip**
  - **Pb: 43.93**
  - **Se: 44.83**
  - **Cd: 11.24**
- **Region 3: Cation exchange region**
  - **Pb: 41.34**
  - **Se: 52.26**
  - **Cd: 6.40**
- **Region 4: Cation exchange region**
  - **Pb: 34.04**
  - **Se: 53.68**
  - **Cd: 12.29**
- **Region 5: PbSe tip**
  - **Pb: 44.30**
  - **Se: 47.46**
  - **Cd: 8.24**
- **Region 6: PbSe tip**
  - **Pb: 45.74**
  - **Se: 46.41**
  - **Cd: 7.84**
- **Region 7: Cation exchange region**
  - **Pb: 39.07**
  - **Se: 54.53**
  - **Cd: 6.39**
- **Region 8: Cation exchange region**
  - **Pb: 40.08**
  - **Se: 52.18**
  - **Cd: 7.74**

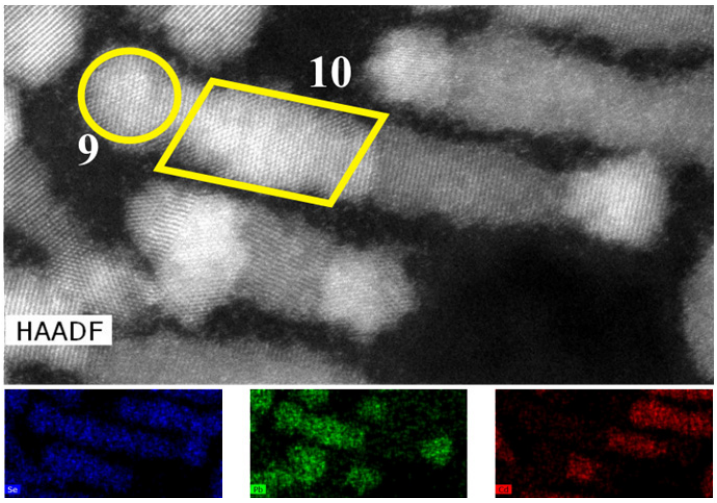

Figure S13. CdSe-PbSe dumbbell NC where some cation exchange was observed.

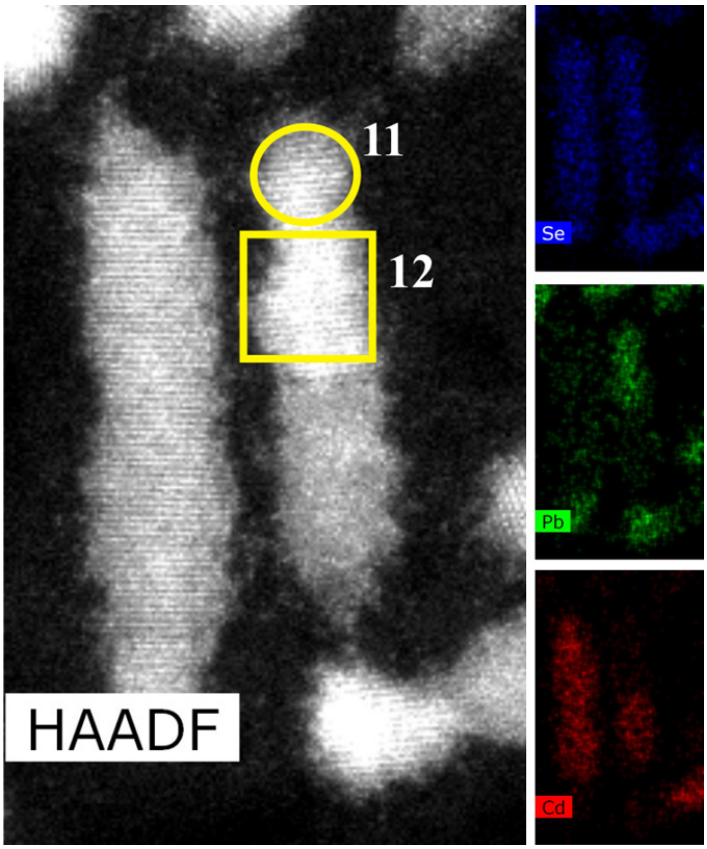

Figure S14. CdSe-PbSe dumbbell NC where some cation exchange was observed.

Atomic percentages:

- **Region 9: PbSe tip**
  - **Pb: 45.42**
  - **Se: 54.45**
  - **Cd: 0.13**
- **Region 10: Cation exchange region**
  - **Pb: 46.19**
  - **Se: 47.65**
  - **Cd: 6.16**
- **Region 11: PbSe tip**
  - **Pb: 38.59**
  - **Se: 54.15**
  - **Cd: 7.26**
- **Region 12: Cation exchange region**
  - **Pb: 41.54**
  - **Se: 52.54**
  - **Cd: 5.92**

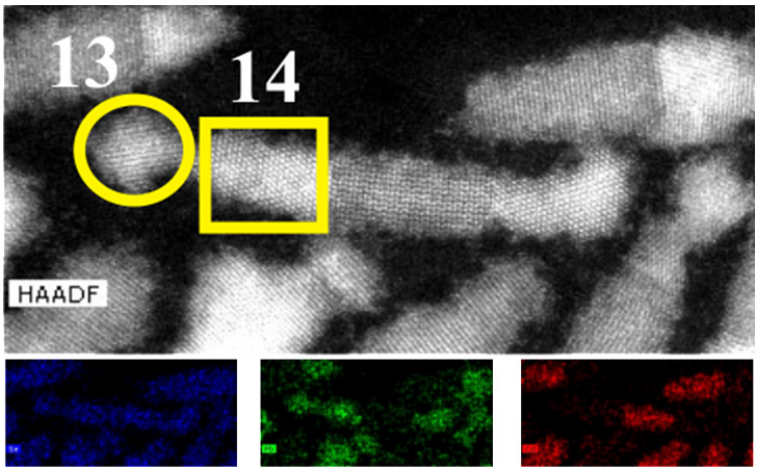

Figure S15. CdSe-PbSe dumbbell NC where some cation exchange was observed.

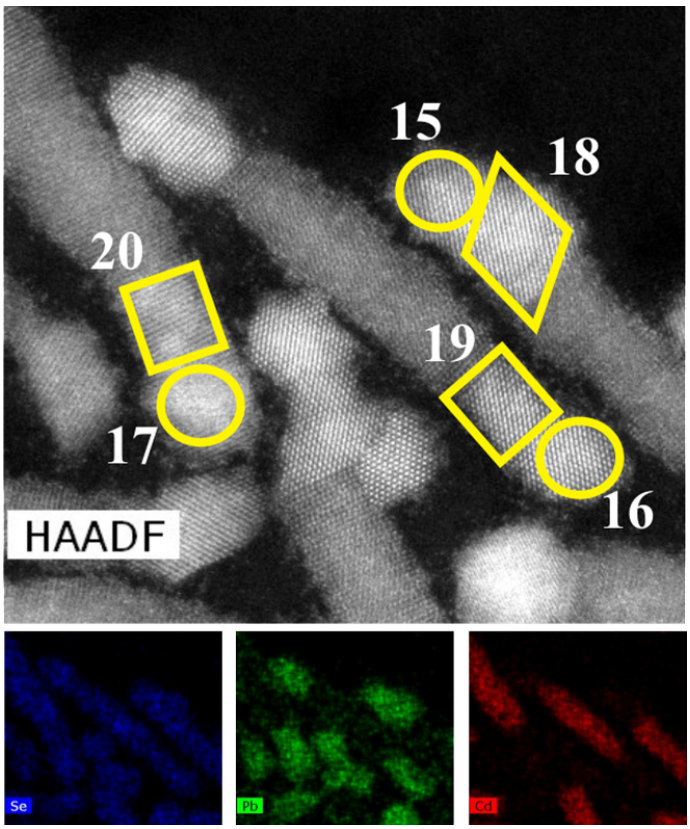

Figure S16. CdSe-PbSe dumbbell NCs where some cation exchange was observed.

Atomic percentages:

- **Region 13: PbSe tip**
  - **Pb: 43.00**
  - **Se: 54.83**
  - **Cd: 2.16**
- **Region 14: Cation exchange region**
  - **Pb: 39.74**
  - **Se: 52.64**
  - **Cd: 7.62**
- **Region 15: PbSe tip**
  - **Pb: 46.01**
  - **Se: 46.01**
  - **Cd: 7.98**
- **Region 16: PbSe tip**
  - **Pb: 48.78**
  - **Se: 44.42**
  - **Cd: 6.80**
- **Region 17: PbSe tip**
  - **Pb: 40.96**
  - **Se: 55.65**
  - **Cd: 3.39**
- **Region 18: Cation exchange region**
  - **Pb: 41.76**
  - **Se: 52.19**
  - **Cd: 6.04**
- **Region 19: Cation exchange region**
  - **Pb: 48.62**
  - **Se: 51.38**
  - **Cd: 0.00**
- **Region 20: Cation exchange region**
  - **Pb: 49.31**
  - **Se: 48.95**
  - **Cd: 1.75**

Table S3. Quantification data of 10 STEM-EDX studies on PbSe tips (Figures S11-S16) from where cation exchange proceeded.

PbSe tips from where cation exchange proceeded			
	Pb	**Se**	**Cd**
Region 1	41.04	45.77	13.19
Region 2	43.93	44.83	11.24
Region 5	44.3	47.46	8.24
Region 6	45.74	46.41	7.84
Region 9	45.42	54.45	0.13
Region 11	38.59	54.15	7.26
Region 13	43	54.83	2.16
Region 15	46.01	46.01	7.98
Region 16	48.78	44.42	6.8
Region 17	40.96	55.65	3.39
Mean	43.777	49.398	6.823
Standard Deviation	2.977721164	4.710158761	3.985337153

Table S4. Quantification data of 10 STEM-EDX studies on nanorod domains (Figures S11-S16) where cation exchange took place.

Nanorod domains where cation exchange took place			
	Pb	**Se**	**Cd**
Region 3	41.34	52.26	6.4
Region 4	34.04	53.68	12.29
Region 7	39.07	54.53	6.39
Region 8	40.08	52.18	7.74
Region 10	46.19	47.65	6.16
Region 12	41.54	52.54	5.92
Region 14	39.74	52.64	7.62
Region 18	41.76	52.19	6.04
Region 19	48.62	51.38	0
Region 20	49.31	48.95	1.75
Mean	42.17	51.80	6.03
Standard Deviation	4.67	2.07	3.33

Nanorod domains where full cation exchange took place: Figures S17-S19. The quantitative analyses were carried out the yellow highlighted regions with numbers.

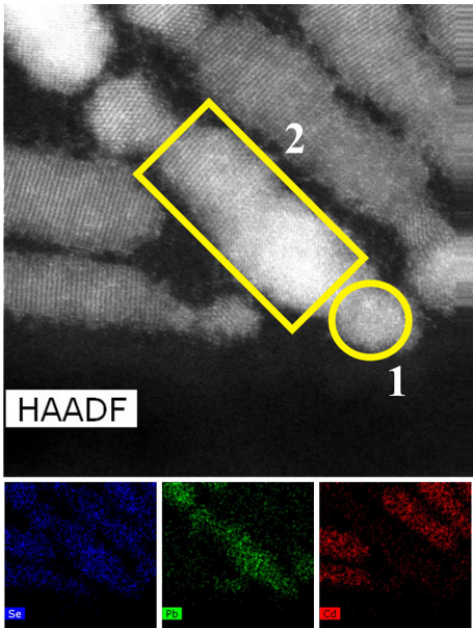

Figure S17. CdSe-PbSe dumbbell NC where full cation exchange was observed. In Supporting Movie S2, it is shown that the cation exchange propagated only from the lower PbSe tip for this NC, numbered as 1 in the figure.

Atomic percentages:

- **Region 1: PbSe tip**
  - **Pb: 44.49**
  - **Se: 55.51**
  - **Cd: 0**
- **Region 2: Nanorod domain where whole nanorod transformed from CdSe to PbSe**
  - **Pb: 43.36**
  - **Se: 53.55**
  - **Cd: 3.09**
- **Region 3: PbSe tip**
  - **Pb: 45.05**
  - **Se: 53.49**
  - **Cd: 1.45**
- **Region 4: Nanorod domain where whole nanorod transformed from CdSe to PbSe**
  - **Pb: 48.40**
  - **Se: 50.91**
  - **Cd: 0.95**

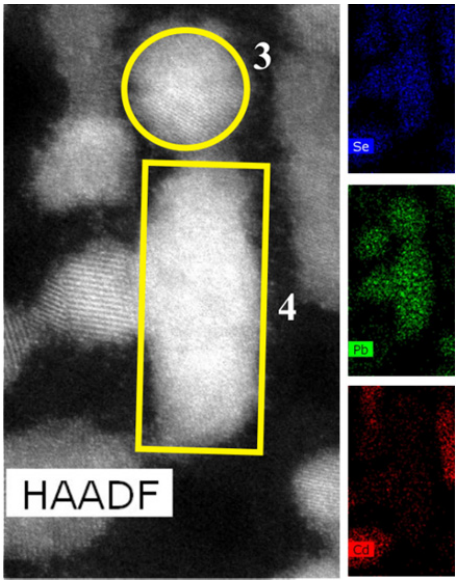

Figure S18. CdSe-PbSe dumbbell NC where full cation exchange was observed.

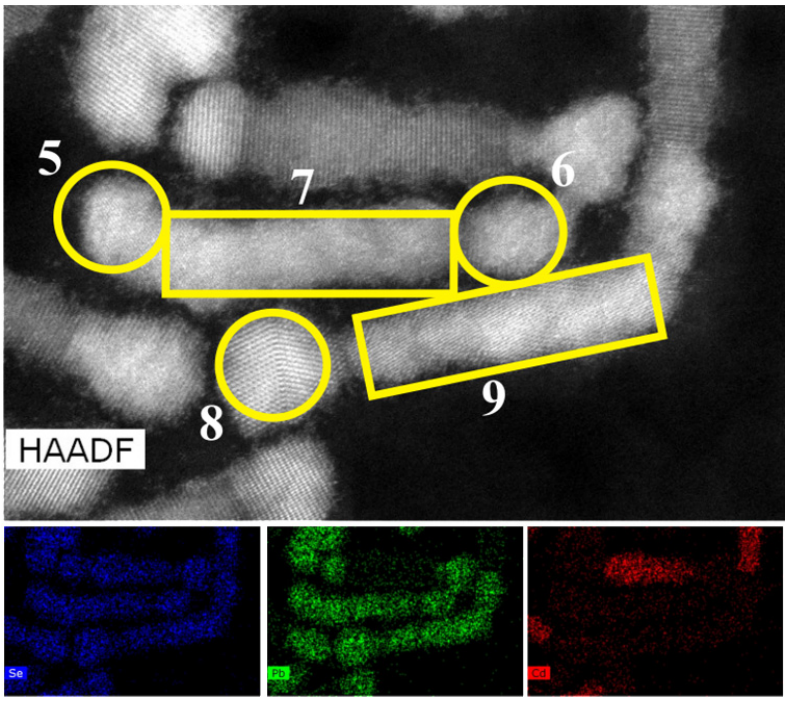

Figure S19. CdSe-PbSe dumbbell NCs where full cation exchange was observed.

Atomic percentages:

- **Region 5: PbSe tip**
  - **Pb: 46.88**
  - **Se: 46.55**
  - **Cd: 6.56**
- **Region 6: PbSe tip**
  - **Pb: 43.79**
  - **Se: 50.65**
  - **Cd: 5.56**
- **Region 7: Nanorod domain where whole nanorod transformed from CdSe to PbSe**
  - **Pb: 44.69**
  - **Se: 47.36**
  - **Cd: 7.95**
- **Region 8: PbSe tip**
  - **Pb: 49.17**
  - **Se: 50.83**
  - **Cd: 0**
- **Region 9: Nanorod domain where whole nanorod transformed from CdSe to PbSe**
  - **Pb: 47.99**
  - **Se: 50.69**
  - **Cd: 1.32**

Table S5. Quantification data of 5 STEM-EDX studies on PbSe tips of nanorods (Figures S17-S19) where nanorod domain totally transformed from CdSe to PbSe.

PbSe tips of nanorod domains where full cation exchange took place			
	Pb (%)	**Se (%)**	**Cd (%)**
Region 1	44.49	55.51	0
Region 3	45.05	53.49	1.45
Region 5	46.88	46.55	6.56
Region 6	43.79	50.65	5.56
Region 8	49.17	50.83	0
Mean	45.89	51.41	2.71
Standard Deviation	2.17	3.38	3.13

Table S6. Quantification data of 4 STEM-EDX studies on nanorods (Figures S17-S19) where the nanorod domain fully transformed from CdSe to PbSe.

Nanorod domains where full cation exchange was observed			
	Pb (%)	**Se (%)**	**Cd (%)**
Region 2	43.36	53.55	3.09
Region 4	48.4	50.91	0.95
Region 7	44.69	47.36	7.95
Region 9	47.99	50.69	1.32
Mean	46.11	50.63	3.33
Standard Deviation	2.47	2.54	3.22

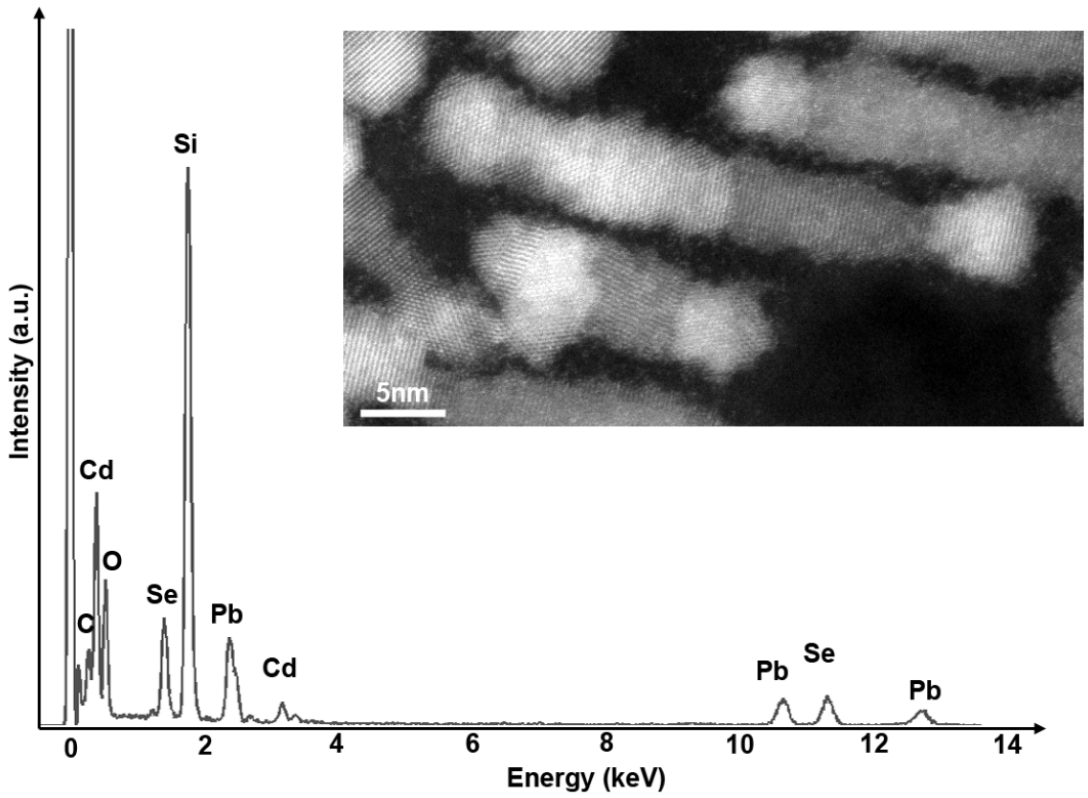

Figure S20. A representative EDS spectrum. The spectrum shown is the sum spectrum of Figure 1h (inset). The Si peak is from the SiN support membrane.

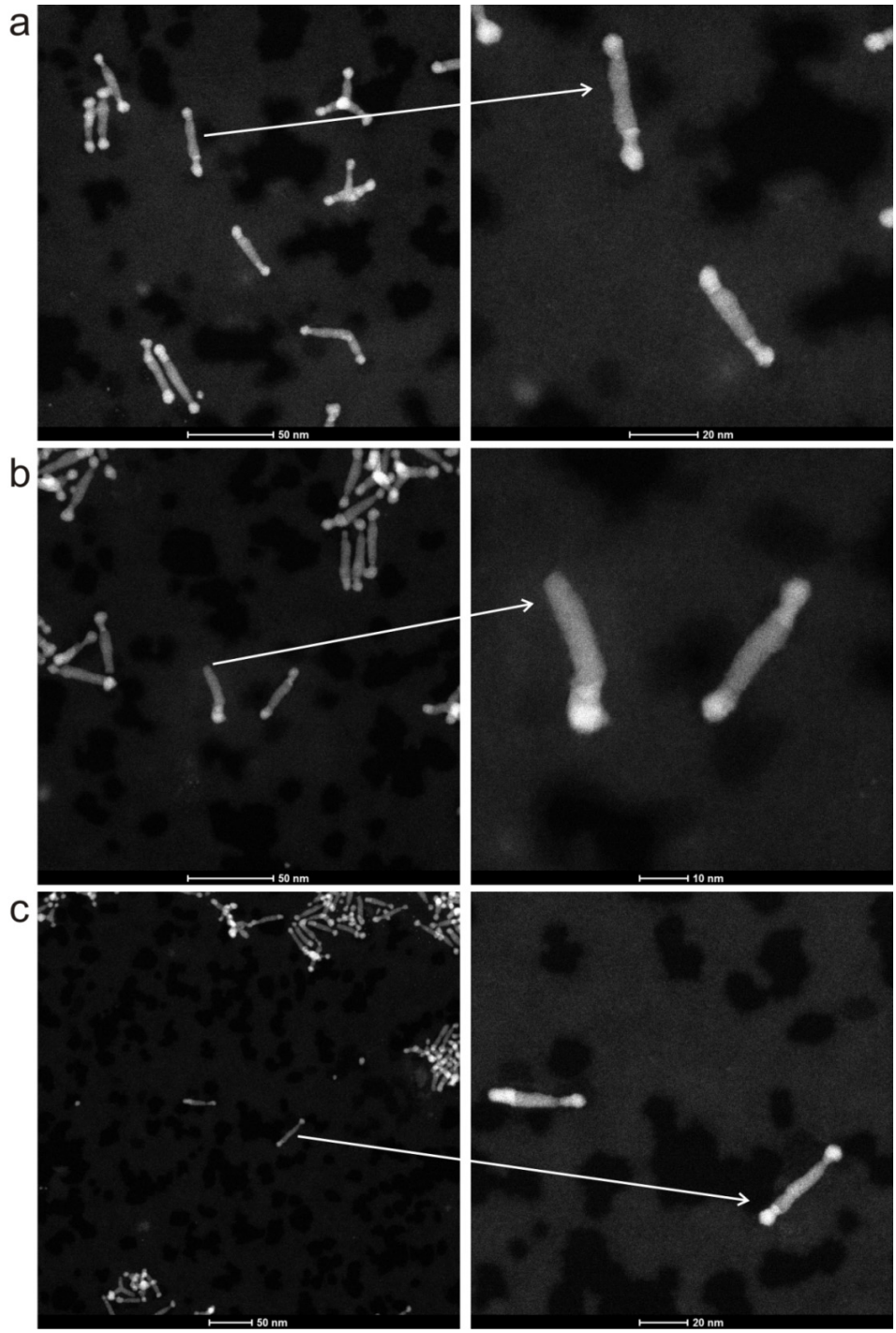

Figure S21. HAADF-STEM images of isolated PbSe-CdSe hetero-nanodumbbells which partially underwent the transformation after heating to a temperature of 200 °C and 5 mins annealing. Overview images are shown at the left-hand side, details of the isolated nanodumbbells are shown at the right-hand side. Heating for longer periods of time did not lead to a full transformation. Heating to higher temperatures led to CdSe sublimation as also shown in Movie S3.

E. Force-field MD simulations

Force field for the Pb-Se-Cd system

There are very few of force fields developed for CdSe and PbSe in the literature. One of the most frequently used force fields for CdSe is developed by Rabani [5] within a Partially Charged Rigid Ion Model (PCRIM) [6] approach. In this force field model, Lennard-Jones (LJ) potentials were used to describe the short-range interactions and effective charges of ±1.18 *e* for Cd and Se ions were obtained by empirical fitting. Schapotschnikow et al. [7] developed a force field for PbSe using the same model to study the morphological evolution of PbSe nanocrystals. In this PbSe force field, the effective charges for Pb and Se ions were ±1.29 *e*, and the parameters of the LJ potential that describe the Se-Se short-range interactions in PbSe were very different from that in the CdSe force field. Therefore, these two force fields cannot be easily combined to describe the Pb-Cd-Se system. To our best knowledge, up to now there was no transferable force field developed for the Pb-Cd-Se system. In this work, a set of transferable pair potentials was derived for the Pb-Se-Cd system. The PCRIM model [6] was chosen to describe the interatomic interactions. Interatomic interactions only contain Coulomb interactions and short-range two-body interactions (Buckingham potential):

$$u_{ij}(r_{ij}) = \frac{q_i q_j}{r_{ij}} + Ae^{-r_{ij}/\rho} - \frac{C}{r_{ij}^6}$$

The first term in this equation is the electrostatic potential, and the second and third terms describe the short-range interactions. r_{ij} is the interatomic distance, q_i is the effective charge, A, ρ, and C are model parameters.

The Bader charge analysis [8] was performed on the results of density functional theory (DFT) calculations on CdSe and PbSe bulk phases in order to determine accurate values of the effective charges on the atoms (See Section F of the SI for computational details of the DFT calculations). The Bader charges of the Cd atoms the wurtzite (WZ), zinc blende (ZB), rock salt (RS), and honeycomb (HC) structures are 0.711, 0.725, 0.825, and 0.750 *e*, respectively, and that of the Pb atoms in the RS, cesium chloride (CsCl), ZB and HC structures are 0.812, 0.813, 0.804, 0.781 *e*, respectively. The value of the effective charges in the force field model were set as q = ±0.8 *e* for both cations and anions. The interatomic short-range interactions between two cations are omitted since the effective ion radii of cations are relatively small. The Buckingham parameters were obtained by fitting to experimental data and DFT simulations. The experimental data includes the lattice parameters, elastic constants, and bulk moduli of CdSe in the WZ and ZB structures and PbSe in the RS structure. The DFT data includes lattice parameters and relative stabilities of four CdSe polymorphs (WZ, ZB, RS, and HC) and four PbSe

polymorphs (RS, CsCl, ZB, and HC). The lattice parameters obtained from DFT calculations were normalized be rescaling their volumes, in which the scale factors for CdSe and PbSe polymorphs were respectively the ratios of the volumes of WZ-CdSe and RS-PbSe computed from DFT divided by the experimental value. The ratios of *c*/*a* from our DFT calculations remained unchanged. Relaxed fitting was used in the fitting procedure in order to achieve a higher quality of fitting. A cut off radius of 12.0 Å was set for all short-range interactions and the Ewald summation [9] was used to calculate the long-range Coulomb interactions in the bulk phases. All calculations in the fitting procedure were carried out by The General Utility Lattice Program (GULP) [10]. The complete parameter set for the Pb-Se-Cd system is listed in Table S7**.**

Table S7. Parameters of the Pb-Se-Cd force field. The effective ion charges q are ±0.8 e. Short-range interactions between cations were not taken into account.

interactions	A (eV)	ρ (Å)	C (eV·Å^6)
Cd-Se	2640000000	0.108	64.4
Pb-Se	4880000	0.173	211
Se-Se	5200	0.384	127

In Table S8 and S9, several physical properties of PbSe and CdSe polymorphs calculated from our Pb-Se-Cd force field are listed, together with available experimental results and DFT computations. Note that the data used in fitting procedure is in bold and the normalized lattice parameters are listed in square brackets. To obtain the lattice parameters and root mean square displacement (RMSD) at 300 K, MD simulations were performed for the WZ-CdSe and RS-PbSe structures. In general, the Pb-Se-Cd force field is able to reproduce quite a wide range of physical properties of CdSe and PbSe polymorphs with considerable accuracy.

Model construction for the PbSe-CdSe nanodumbbells

Two different PbSe/CdSe interfaces were observed in the dumbbell NCs by HREM: {100}PbSe/{0001}CdSe and {111}PbSe/{0001}CdSe. The former is a non-polar/polar interface and the latter is a polar/polar interface. The polarization of the CdSe rods and PbSe tips cannot be distinguished by the HREM data. Therefore, we assumed that all possible combinations of the four facets existed in the specimen: {100}PbSe/Se-{0001}CdSe, {100}PbSe/Cd-{$000\bar{1}$}CdSe, Pb-{$\bar{1}\bar{1}\bar{1}$}PbSe/Se-{0001}CdSe, and Se-{111}PbSe/Cd-{$000\bar{1}$}CdSe.

Table S8. Physical properties of CdSe calculated by lattice statics (LS) and MD simulations, compared to experimental and DFT data. Lattice parameters a and c are in Å; u is the internal coordinate; the elastic constants c_{ij} and bulk moduli B are in GPa; the lattice energy E_{latt} and energy difference ΔE are in eV/f.u.; the transition pressure P_T is in GPa; the RMSD ξ is in Å; the surface energy E_{surf} is in J/m^2. The values in parentheses are MD results at 300 K; the values in square brackets are normalized lattice parameters from DFT calculations; the values in bold are data used for the fit of the force field parameters.

CdSe	Exp.[a]	PCRIM	DFT[b]
Wurtzite, space group $P6_3mc$ (No. 186)			
a	**4.30**	4.32 (4.36)	4.39
c	**7.01**	6.94 (7.00)	7.17
u	**0.376**	0.379	0.375
c_{11}	**74.1**	72.4	80
c_{12}	**45.2**	47.9	47
c_{13}	**39.0**	41.4	40
c_{33}	**84.3**	72.5	92
c_{44}	**13.4**	12.3	15
c_{66}	**14.5**	12.2	17
B	**53.1**	53.1	60
E_{latt}	-	-6.026	-
P_T (WZ→RS)	3.0	4.1	2.2
ξ_{Cd}	0.14	(0.32)	-
ξ_{Se}	0.13	(0.29)	-
$E_{surf}\{11\bar{2}0\}$	-	0.26	0.50
$E_{surf}\{10\bar{1}0\}$	-	0.25	0.46
Zinc blende, space group $F\bar{4}3m$ (No. 216)			
a	6.08	6.08	6.21 [**6.08**]
c_{11}	**66.7**	61.6	88.1
c_{12}	**46.3**	48.8	53.6
c_{44}	**22.3**	20.3	27.4
B	**53.1**	53.1	65.1
$\Delta E_{ZB\text{-}WZ}$	-	0.014	**-0.002**
Rock salt, space group $Fm\bar{3}m$ (No. 225)			
a	-	5.63	5.75 [**5.63**]
$\Delta E_{RS\text{-}WZ}$	-	0.291	**0.290**
Honeycomb, space group $P6_3/mmc$ (No. 194)			
a	-	4.57	4.66 [**4.56**]
c	-	5.63	6.07 [**5.94**]
$\Delta E_{HC\text{-}WZ}$	-	0.149	**0.211**

[a] The lattice parameters, elastic constants, and bulk moduli of WZ- and ZB-CdSe are reported in Ref. 11; the transition pressure of the WZ→RS transition is reported in Ref. 12; the RMSD of CdSe is reported in Ref. 13. [b] The elastic constants and bulk modulus for WZ- and ZB-CdSe are reported in Ref. 14,15; the transition pressure of the WZ→RS transition is reported in Ref. 16.

Table S9. Physical properties of PbSe calculated by lattice statics (LS) and MD simulations, compared to experimental and DFT data. Lattice parameters a and c are in Å; u is the internal coordinate; the elastic constant c_{ij} and bulk modulus B are in GPa; lattice energy E_{latt} and energy difference ΔE are in eV/f.u.; the transition pressure P_T is in GPa; the RMSD ξ is in Å; the surface energy E_{surf} is in J/m^2. The values in parentheses are MD results at 300 K; the values in square brackets are normalized lattice parameters from DFT calculations; the values in bold are data used for the fit of the force field parameters.

PbSe	Exp.[a]	PCRIM	DFT[b]
Rock salt, space group $Fm\bar{3}m$ (No. 225)			
a	**6.12**	6.09 (6.13)	6.21
c_{11}	**123.7**	129.9	123.6
c_{12}	**19.3**	16.5	12.2
c_{44}	**15.9**	16.5	17.6
B	**54.1**	54.3	49.2
E_{latt}	-	-6.079	-
P_T, (RS→CsCl)	16.0	15.6	18.8
ξ_{Pb}	0.13	(0.27)	-
ξ_{Se}	0.12	(0.24)	-
E_{surf} {100}	-	0.29	0.18
E_{surf} {110}	-	0.49	0.32
Cesium chloride, space group $Pm\bar{3}m$ (No. 221)			
a	-	3.71	3.77 [**3.72**]
$\Delta E_{CsCl-WZ}$	-	0.528	**0.478**
Zinc blende, space group $F\bar{4}3m$ (No. 216)			
a (Å)	-	6.84	6.89 [**6.80**]
ΔE_{ZB-WZ}	-	0.381	**0.374**
Honeycomb, space group $P6_3/mmc$ (No. 194)			
a	-	5.18	5.21 [**5.14**]
c	-	6.05	6.23 [**6.15**]
ΔE_{HC-WZ}	-	0.397	**0.320**

[a] The lattice parameters, elastic constants, and bulk moduli of RS-PbSe are reported in Ref. 17; the transition pressure of the RS→CsCl transition is reported in Ref. 18; the RMSD of PbSe is reported in Ref. 19. [b] The elastic constants and bulk modulus for RS-PdSe is reported in Ref. 20; the transition pressure of the RS→CsCl transition is reported in Ref. 21.

Four nano-dumbbell models were constructed (Figure S22) mimicking the structures, morphologies, and the interfaces of the nano-dumbbells observed experimentally. Model 1 has two non-polar/polar interfaces and Model 2 has two polar/polar interfaces. Both model 3 and 4 have one non-polar/polar interface and one polar/polar interface, but their polarizations are anti-parallel. All nano-dumbbell models were made of a WZ-CdSe rod and two RS-PbSe tips. A CdSe rod consists of 3219 CdSe pairs with a length of about 11.0 nm and a diameter of about 4.2 nm, and a PbSe tips consists of 1381 PbSe pairs with a diameter of

about 4.5 nm. We tailored the CdSe rod and the PbSe tips to mimic the "necks" of the CdSe rods at the PbSe/CdSe interfaces and the morphology of the PbSe tips observed experimentally (see Figure 1 in the main text). The CdSe rods are identical in the four models while the PbSe tips have slightly differences in morphology and surface. The surfaces $\{10\bar{1}0\}$CdSe, $\{11\bar{2}0\}$CdSe, {100}PbSe, and {110}PbSe are exposed most to vacuum. These are the most stable surfaces in WZ-CdSe and RS-PbSe with the lowest surface energies. Initially, the orientations of the CdSe rods and the PbSe tips with different types of interfaces were set as same as the nano-dumbbell in Figure 2c of the main text, and the initial distance between the PbSe and CdSe interfaces was set as ~3.0 Å.

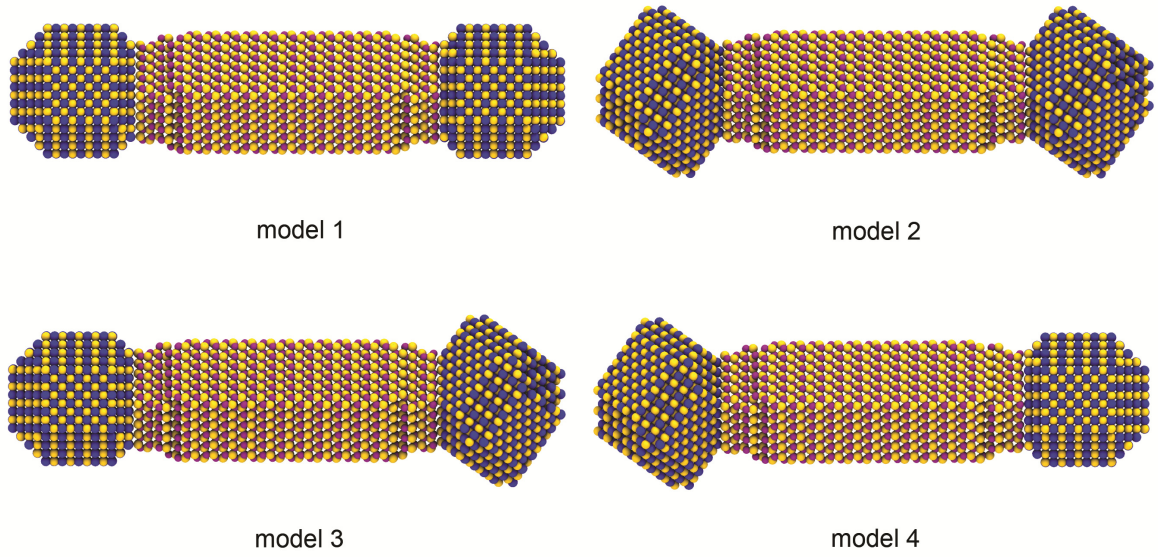

Figure S22. Four PbSe-CdSe dumbbell configurations (models 1, 2, 3, and 4) having different PbSe/CdSe interfaces. The yellow, purple, and blue spheres are Se, Cd, and Pb atoms, respectively.

Molecular dynamics simulations results for Model 1, 2, and 4

For the MD simulations, Coulombic and short-range interactions were calculated by taking into account all atom pairs using the newly developed force field potential set given above in Table S7. Figure S23 shows the final configurations of the PbSe/CdSe nano-dumbbell model 1, 2, and 4 after MD simulations at 500 K for 5 ns.

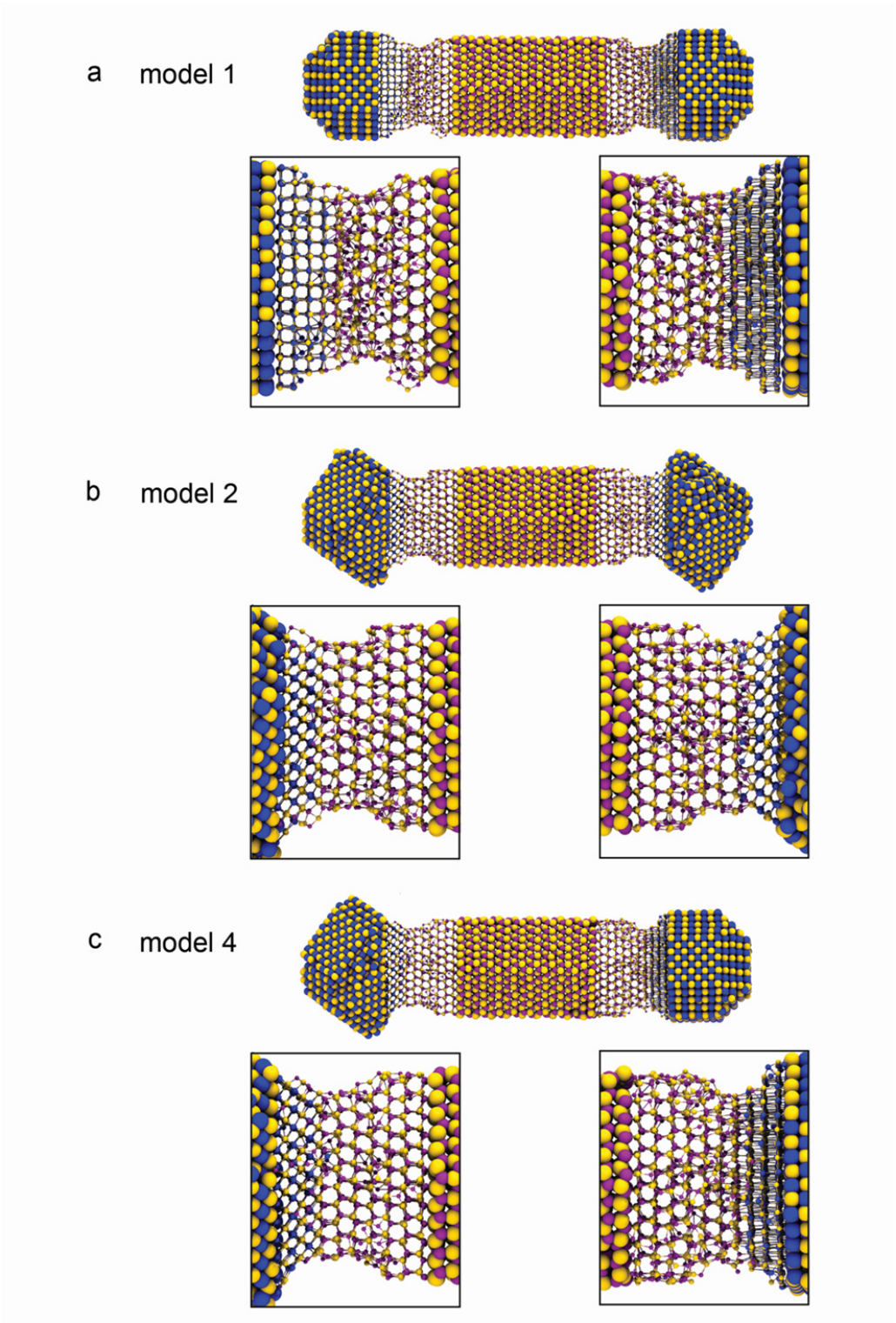

Figure S23. (a,b,c) Final configuration of PbSe-CdSe dumbbell model 1, 2, and 4 after MD simulations at a temperature of 500 K for 5 ns. The ball-stick presentation was used to show the structure of the interfaces. The yellow, purple, and blue spheres are Se, Cd, and Pb atoms, respectively. Interfaces are magnified for closer inspection.

Figure S24 shows the {001}PbSe and {0001}CdSe atomic bilayers parallel to the PbSe/CdSe interface at the left-hand side of model 3 shown in Figure 3 of the main text. Figure S25 shows the maps of root-mean-squared displacement (RMSD) for each atom in the model 1, 2, and 4. Similar results as nano-dumbbell model 3 were obtained: All models are structurally and morphologically stable at temperatures up to 500 K in a simulation time of 5 ns. Structural disorder of the surface atoms in the CdSe domains was found near the polar/polar interfaces; stronger structural disorder was found in the CdSe domains near the non-polar/polar interfaces. Cd atoms near the interfaces have an abnormally high mobility compared to the other atoms. According to our simulations, the structural disorder in the CdSe domains and the high mobility of Cd atoms are strongly influenced by the heterostructural interfaces.

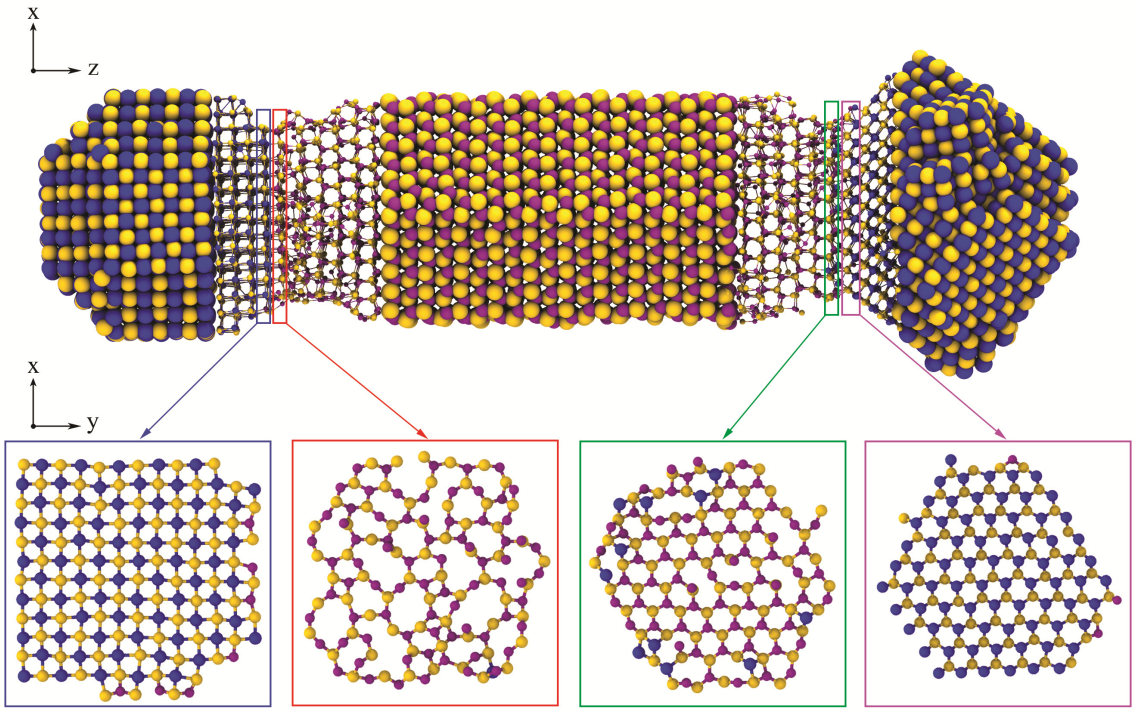

Figure S24. Details of the PbSe/CdSe interfaces for model 3, shown in Figure 3(a-c) in the main text. The yellow, purple, and blue spheres are Se, Cd, and Pb atoms, respectively. Bottom: planar views of the first (001)PbSe bilayers, and the first (0001)CdSe bilayers at the interfaces. The first (0001)CdSe bilayers contain vacancies, which likely enhances the atomic mobility in these layers. It is clear that the number of vacancies at the non-polar/polar PbSe/CdSe interface (left-hand side) is larger than in the number of vacancies in the polar/polar PbSe/CdSe interface (right-hand side).

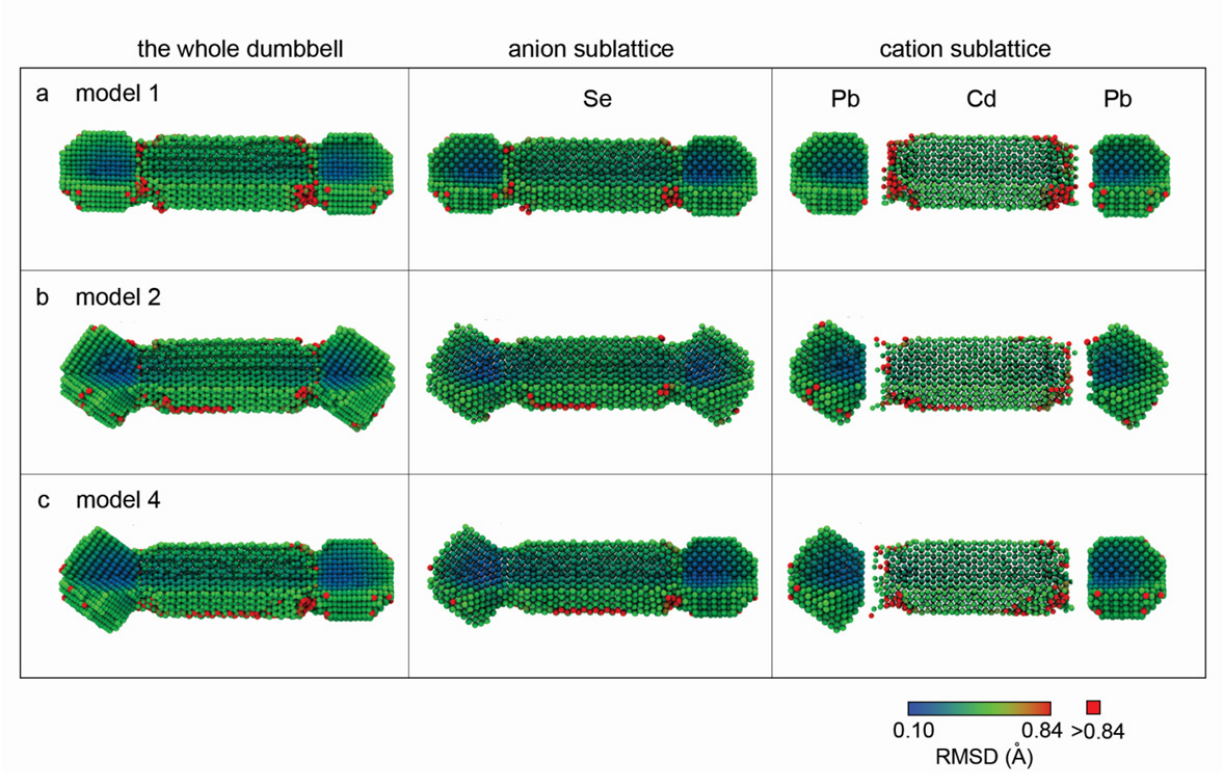

Figure S25. (a,b,c) The map of the root-mean-squared displacement (RMSD) for each atom for the PbSe-CdSe dumbbell model 1, 2, and 4 at 500 K. The columns from left to right are the whole PbSe-CdSe dumbbells, the anion sublattices, and the cation sublattices, sequentially. The dumbbells are cut so that both of the surface and inner atoms can be seen. The pure red atoms correspond to those have a RMSD larger than 0.84 Å.

F. Density Functional Theory (DFT) calculations

F1. Defect energy calculations

All calculations were carried out using the first-principles' Vienna *Ab initio* Simulation Program (VASP) [22,23] employing density functional theory (DFT) within the Projector-Augmented Wave (PAW) method [24]. The generalized gradient approximation (GGA) formulated by Perdew, Burke, and Ernzerhof (PBE) [25] was employed for the exchange and correlation energy terms. The cut-off energy of the wave functions was 350.0 eV. The cut-off energy of the augmentation functions was about 500.0 eV. The electronic wave functions were sampled on a 4×4×2 grid using the Monkhorst and Pack method with 8 to 20 *k*-points depending on different symmetries of super-cells (108 atoms). Structural optimizations were performed for both lattice parameters and coordinates of atoms. Different *k*-meshes and cut-off energies for waves were tested to have a good convergence (< 2 meV/atom).

In order to have a better comparison and to exclude the differences of configurational entropies caused by different cell-sizes and number of atoms, the FCC lattice of WZ PbSe was transferred into a hexagonal cell with the relationships: $a_h = 3/\sqrt{2}\ a_c$, $c_h = 2\sqrt{3}\ a_c$, here (a_c is the lattice parameter of the cubic face, a_h, c_h are the lattice parameters of the hexagonal cells). In this way, one hexagonal super-cell (from FCC lattice) contains 54 Pb and 54 Se atoms, with dimensions of $3a_h \times 3a_h \times 2c_h$. A super-cell for the HCP CdSe cell is built by $a^*_h = 3\ a_h$, $c_h = 3\ a_c$, which contains the same amounts of Cd and Se atoms but in a different order of stacking. Point defects including Schottky defects, Frenkel defects, and the substitutional Pb-Cd defect were considered in this study. If there were two point defects in the supercell, the defect sites were placed as far as possible from each other within the supercell, in order to avoid artificial interaction between the defect sites.

The *Schottky defect* is composed of one cation vacancy and one anion vacancy. We calculated two configurations: the Schottky dimer and Schottky pair. In the dimer, the cation vacancy and the anion vacancy are occupying adjacent lattice sites: the two vacancies are bound. In the Schottky pair, the two vacancy species are separated (as much as possible within the periodic supercell). The formation energy is defined as

$$E_f = E(M_{53}Se_{53}) - {}^{53}\!/_{54}\, E(M_{54}Se_{54}).$$

Here, the perfect cell is used as the reference phase.

A *Frenkel defect* is a defect whereby one atom has left its lattice site in the cell, therefore it consists of one vacancy and one interstitial of the same atomic species. Both cation and anion Frenkel defects are included. The formula for the Frenkel defect formation energy is :

$$E_f = E(M_{54}Se_{54})_{Frenkel} - E(M_{54}Se_{54})_{perfect},$$

which is simply the energy difference between the defective cell and the perfect cell.

The *(Cd, Pb) substitutional defect energy* is the energy required to swap a Pb atom and a Cd atom; the Cd atom occupies a Pb site in the PbSe lattice and the Pb atom occupies a Cd site in the CdSe lattice. The formation energy is defined with respect to the perfect CdSe and PbSe supercells as follows:

$$E_f = E(Cd_{53}PbSe_{54}) + E(CdPb_{53}Se_{54}) - [E(Cd_{54}Se_{54}) + E(Pb_{54}Se_{54})],$$

with $E(Cd_{53}PbSe_{54})$ and $E(CdPb_{53}Se_{54})$ the energy of super-cells containing one substituted cation atom, and $E(Cd_{54}Se_{54})$ and $E(Pb_{54}Se_{54})$ the energy of perfect super-cells. The results are shown in Table S10.

Table S10. Defect energies (in eV) in MSe (M=Cd,Pb) calculated using DFT-GGA-PBE. A Schottky defect consists of a cation vacancy and an anion vacancy, while a Frenkel defect consists of a vacancy and an interstitial atom of the same species.

Defect		Formation energy E_{defect} (eV)	
		CdSe	PbSe
Schottky pair	$V_M + V_{Se}$	4.82	1.52
Schottky dimer	$\{V_M V_{Se}\}$	2.02	1.24
Frenkel cation	$V_M + M^i$	3.16	3.30
Frenkel anion	$V_{Se} + Se^i$	6.00	3.80
Substitutional cation	$[Cd]_{Pb}+[Pb]_{Cd}$	0.98	

From Table S10, it becomes clear that PbSe is a typical Schottky material, as the Schottky defect energies are much lower than the Frenkel defect energies. Consequently, only vacancies, and no interstitial atoms will be present. In CdSe, the lowest defect energy is for the Schottky dimer, however the dimer is likely not mobile and will therefore not participate in the cation exchange. The second-lowest energy is that of the Cd Frenkel defect (Cd vacancy and Cd interstitial). As the "Cd interstitial" evaporates into the vacuum, the Cd vacancy is left behind and is then available to mediate the cation exchange, as depicted schematically in Figure S1.

Finally we would like to make a few remarks on the interpretation of the defect energy calculations. The defect energies listed in Table S10 are for defects in bulk CdSe and PbSe at thermal equilibrium. The absolute values of the defect energies in Table S10 are rather high. The equilibrium atomic concentration of defects can be evaluated as $f_{defect}=\exp(-E_{defect}/k_BT)$ where k_B is the Boltzmann constant and T is the temperature in K. Therefore, a defect energy of 1.24 eV for the Schottky dimer in PbSe leads to an atomic fraction of $f_{V\{PbSe\}}=7.1\cdot10^{-15}$ at a temperature of 443 K. Considering that the number of atoms in the nano-dumbbells is approximately 30,000, thermodynamically the number of vacancies to be expected is zero. It is clear also from the high mobility of the Cd atoms near the interface shown in Figure 3 that bulk defect calculations cannot be directly applied to nanoscale materials with surfaces and interfaces: the formation energies of defects at surfaces and interfaces is apparently an order of magnitude lower than in the bulk.

F2. Energies of PbSe-CdSe mixed phases

In order to investigate the energetics of mixing into more detail, the DFT-PAW-GGA-PBE approach as implemented in the VASP code [22-25] was also applied to mixed PbSe-CdSe phases. The formation energy (for a temperature of 0 K and a pressure of 0 Pa) was defined with respect to the lowest-energy phases: RS PbSe and WZ CdSe, as

$$\Delta E\{Pb_xCd_{1-x}Se\}_{RS/WZ}=E\{Pb_xCd_{1-x}Se\}_{RS/WZ}-xE\{PbSe\}_{RS}-(1-x)E\{CdSe\}_{WZ} \quad (1)$$

Here ΔE and E are expressed in eV per formula unit, while x is the atomic fraction of Pb atoms amongst the cations. The result for 0 K is shown in Fig. S26. At this temperature, all formation energies are positive, indicating complete phase separation.

At elevated temperatures, configurational entropy becomes a contributing term in the Gibbs free energy. The $(Cd_{1-x}Pb_x)Se$ phases can be considered as an CdPb alloy on the metal sublattice. For a random model the configurational entropy is $S = -k_B\{x\ln(x) + (1-x)\ln(1-x)\}$, where k_B is the Boltzmann constant. The Gibbs free energy $G(T)$ at p=0 Pa for $(Cd_{1-x}Pb_x)Se$ is then evaluated as

$$G(T) = E(0) - TS = E(0) + Tk_B\{x\ln(x) + (1-x)\ln(1-x)\} \quad (2)$$

where $E(0)$ is the formation energy at 0 K. For temperatures up to 500 K, the contribution of TS to the Gibbs free energy is always less than 0.03 eV (of the order of kT) and does not change the characteristics of the relative stability shown in Figure S26.

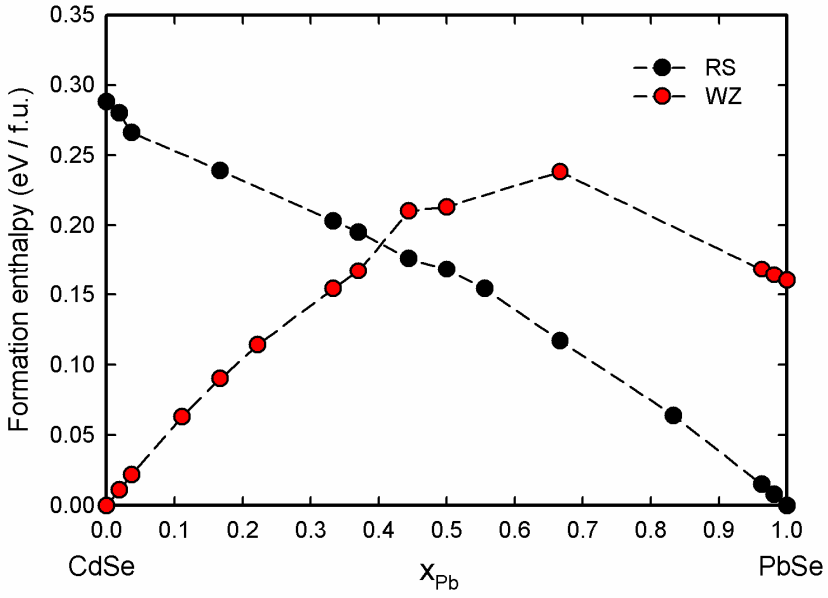

Figure S26. The formation enthalpy ΔE (meV per formula unit) for various $(Pb_xCd_{1-x})Se$ phases. Red circles show the energies of the WZ-based structures, black spheres the energies of the RS-based structures. Lines are drawn to guide the eye.

From Figure S26 it follows that below a Pb cation concentration of 40 at.%, the WZ phase is favoured, while above that concentration the RS phase is favoured. However, because formation enthalpy is positive for the entire compositional range (not only at 0 K but also for temperatures up to 500 K), mixing is not favourable and phase separation into RS PbSe and WZ CdSe will always occur. This is in good agreement with the MD simulations (Figures 3, S23-S25) and with the experiments, where only a low degree of mixing was observed (Table S1).

Table S11. Calculated results for ternary $(Cd_{1-x}Pb_x)Se$ phases using DFT-GGA approach. The lattice parameters and formation energy ΔE are calculated for a range of compositions with of values of the Pb cation concentration $0 \leq x \leq 1$, both for the rock salt (RS) phase and the wurtzite (WZ) phase.

	RS			WZ			
x	A (Å)	E (eV/f.u.)	ΔE (eV/f.u.)	a(Å) / c (Å)	c/a	E (eV/f.u.)	ΔE (eV/f.u.)
0.00	5.736	-5.361	+0.288	4.381 / 7.155	1.633	-5.651	0.00
0.0185	5.744	-5.418	+0.280	4.390 / 7.169	1.633	-5.688	+0.011
0.0370	5.771	-5.480	+0.266	4.402 / 7.182	1.632	-5.723	+0.022
0.1111	-	-	-	4.429 / 7.249	1.637	-5.873	+0.063
0.1667	5.830	-5.839	+0.239	4.464 / 7.262	1.637	-5.988	+0.090
0.2222	-	-	-	4.517 / 7.203	1.595	-6.106	+0.114
0.3333	5.893	-6.302	+0.203	4.566 / 7.224	1.582	-6.351	+ 0.154
0.3704	5.915	-6.402	+0.195	4.581 / 7.267	1.586	-6.433	+0.167
0.4444	5.956	-6.614	+0.176	4.611 / 7.178	1.557	-6.581	+0.210
0.5000	5.979	-6.774	+0.168	4.597 / 7.146	1.554	-6.840	+0.213
0.5556	6.003	-6.921	+0.154				
0.6667	6.066	-7.243	+0.117	4.844 / 7.242	1.495	-7.122	+0.238
0.8333	6.134	-7.723	+0.064				
0.9630	6.188	-8.104	+0.015	5.201 / 6.227	1.197 [a)]	-7.951	+0.168
0.9815	6.197	-8.159	+0.008	5.191 / 6.231	1.200 [a)]	-8.003	+0.164
1.000	6.206	-8.214	0.000	5.212 /6.233	1.196 [a)]	-8.054	+0.160

[a)] Relaxation into a metastable structure wherein the atoms have 5-fold coordination.

References

1. Gur, I.; Fromer, N. A.; Geier, M. L.; Alivisatos, A. P. *Science* **2005**, *310*, 462-465.
2. Peng, Z. A.; Peng, X. *J. Am. Chem. Soc.* **2002**, *124*, 3343-3353.
3. Kudera, S.; Carbone, L.; Casula, M. F.; Cingolani, R.; Falqui, A.; Snoeck, E.; Parak, W. J.; Manna, L. *Nano Lett.* **2005**, *5*, 445-449.
4. Carbone, L.; Kudera, S.; Giannini, C.; Ciccarella, G.; Cingolani, R.; Cozzoli P. D.; Manna, L. *J. Mater. Chem.* **2006**, *16*, 3952-3956.
5. Rabani, E. *J. Chem. Phys.* **2002**, *116*, 258.
6. Tsuneyuki, S.; Tsukada, M.; Aoki, H.; Matsui, Y. *Phys. Rev. Lett.* **1988**, *61*, 869.
7. Schapotschnikow, P.; van Huis, M. A.; Zandbergen, H. W.; Vanmaekelbergh, D.; Vlugt, T. J. H. *Nano Lett.* **2010**, *10*, 3966-3971.
8. Bader, R. F. W. *Atoms in Molecules - A Quantum Theory*; Oxford University Press: Oxford, 1990.
9. Ewald P. P. *Ann. Phys.* **1921**, *369*, 253-287.
10. Gale, J. D.; Rohl, A. L. *Mol. Simul.* **2003**, *29*, 291-341.
11. Sadao, A. *Properties of Group-IV, III-V and II-VI Semiconductors*; Wiley: New York, 2005.
12. Yu, W. C.; Gielisse, P. J. *Mater. Res. Bull.* **1971**, *6*, 621-638.
13. Yoshiasa, A.; Koto, K.; Maeda, H.; Ishii, T. *Jpn. J. Appl. Phys.* **1997**, *36*, 781-784.
14. Sarasamak, K.; Limpijumnong, S.; Lambrecht, W. R. L. *Phys. Rev. B* **2010**, *82*, 035201.
15. Deligoz, E.; Colakoglu, K.; Ciftci, Y. *Physica. B, Condens. Matter* **2006**, *373*, 124-130.
16. Sarasamak, K.; Kulkarni, A. J.; Zhou, M.; Limpijumnong, S. *Phys. Rev. B* **2008**, *77*, 024104.
17. Landolt-Börnstein, *Semiconductors, Group IV Elements, IV-IV and III-V Compounds. Landolt-Börnstein, New Series, 41*; Springer: Berlin, 2005.
18. Ovsyannikov, S. V.; Shchennikov, V. V.; Manakov, A. Y.; Likhacheva, A. Y.; Ponosov, Y. S.; Mogilenskikh, V. E.; Vokhmyanin, A. P.; Ancharov, A. I.; Skipetrov, E. P. *Phys. Status Solidi B* **2009**, *246*, 615-621.
19. Noda, Y.; Masumoto, K.; Ohba, S.; Saito, Y.; Toriumi, K.; Iwata, Y.; Shibuya, I. *Acta Cryst.* **1987**, *C43*, 1443-1445.
20. Zhang, Y.; Ke, X.; Chen, C.; Yang, J.; Kent, P. R. C. *Phys. Rev. B* **2009**, *80*, 024304.
21. Bencherif, Y.; Boukra, A.; Zaoui, A.; Ferhat, M. *Mater. Chem. Phys.* **2011**, *126*, 707-710.
22. Kresse, G.; Hafner, J. *Phys. Rev. B* **1993**, *47*, 558.
23. Kresse, G.; Furthmüller, J. *J. Comput. Mat. Sci.* **1996**, *6*, 15-50.
24. Kresse, G.; Joubert, D. *Phys. Rev. B* **1999**, *54*, 1758.
25. Perdew, J. P.; Burke, K.; Ernzerhof, M. *Phys. Rev. Lett.* **1996**, *77*, 3865.